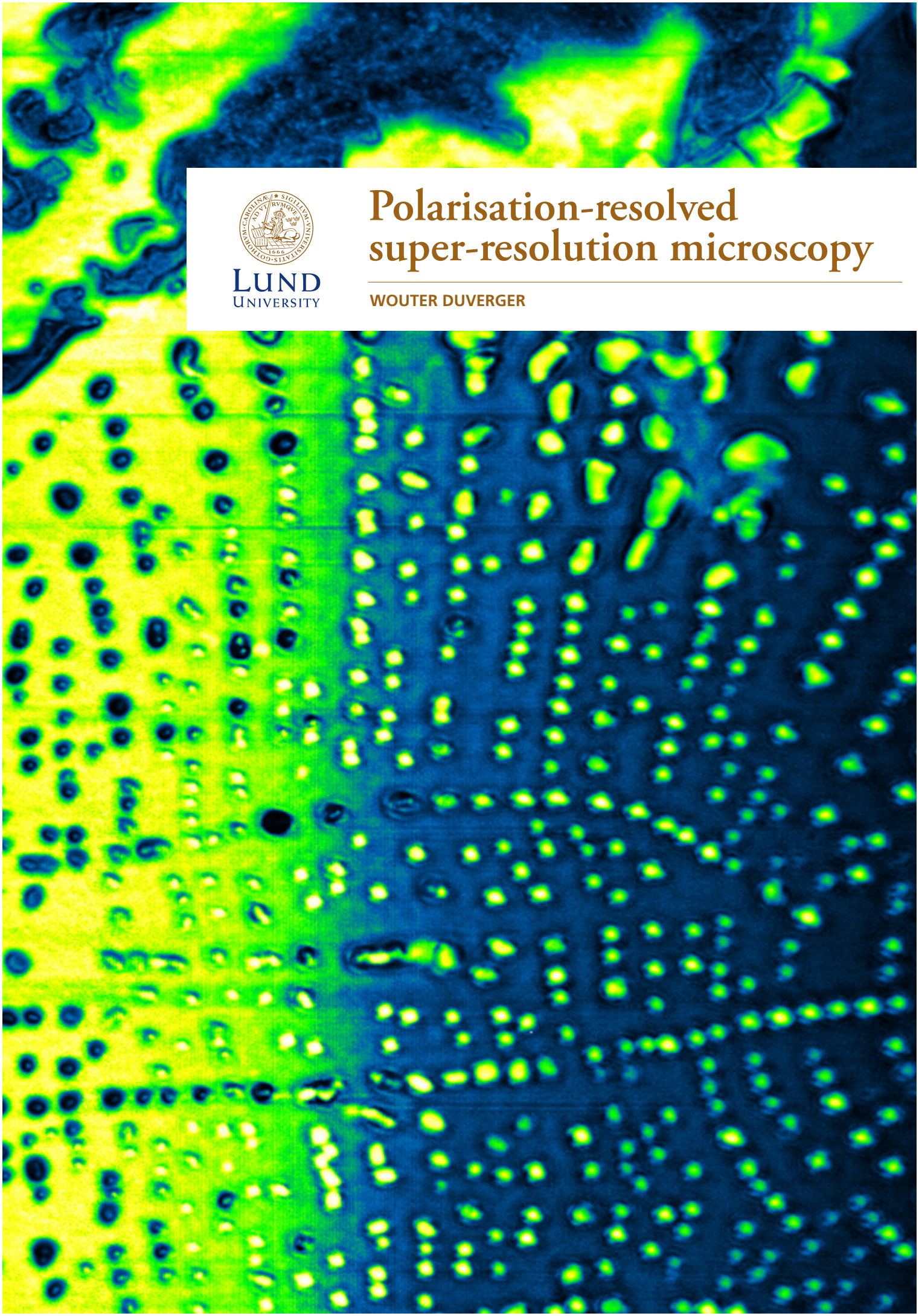

LUND UNIVERSITY

Polarisation-resolved super-resolution microscopy

WOUTER DUVERGER

Polarisation-resolved super-resolution microscopy

by

Wouter Duverger

In partial fulfilment of the requirements for the degree of

MSc in Physics
Biological Physics and Computational Biology,

at the NanoLund Centre for Nanoscience, Lund University,
to be defended publicly on (May 20, 2021).

Project duration	4 months (full-time equivalent)
Supervision	prof. dr. Jonas Tegenfeldt
Daily supervision	dr. Jason Beech
Examiner	prof. dr. Edouard Berrocal

LUND UNIVERSITY

NANOLUND

NANOTECHNOLOGY FOR THE FUTURE

Abstract

(to do)

Contents

Nomenclature

APD	Avalanche photodetector
AOM	Acousto-optical modulator
HWP	Half-wave plate
MPE	Maximum permissible exposure
OD	Optical density (an OD2 filter reduces the light intensity by a factor of 10^2)
PMT	Photomultiplier tube
PSF	Point spread function
pSTED	Polarisation-resolved stimulated emission depletion microscopy
QWP	Quarter-wave plate
SLM	Spatial light modulator
STED	Stimulated emission depletion microscopy
TCSPC	Time-correlated single photon counter

1 Background

(Why do we want to see small things?)

Microscopy - imaging structures at microscopic scales - is an extremely wide and varied field. It is widely accepted to have began in the sixteen-hundreds, with Antoni van Leeuwenhoek's discovery of bacteria and other single-celled organisms (ref). After that, microscopes have been getting higher resolution, but as lenses got better and better, they were not the resolution bottleneck any more. Specifically, in 1873, Ernst Abbe determined that the best possible focus that a microscope can reach is limited by the wavelength of the light used (ref). This meant that the microscopes of the time were limited to a resolution of roughly 400 nm (assuming focused visible white light). It was long believed that the Abbe limit was a fundamental limit of nature, and that the only way around it was by using light of a different wavelength. This is one of the reasons for the development of electron microscopes (ref), as quantum mechanics postulates that accelerated electrons have much shorter wavelength than visible light.

1.1. Diffraction-limited microscopy

(Fluorescence microscopy is great, but was limited in resolution until recently.) I will discuss two ways to get around this problem. The first is indirect and requires playing with a new aspect of light (polarisation) that allows you to get information about structures that you cannot see. The second (STED microscopy) directly increases the image resolution. The excitation light is still limited to the Abbe limit, but we add another laser to effectively improve our focusing.

1.2. Polarisation microscopy

The wave nature of light might limit the resolution of a microscope, but it can also be exploited in our favour. Light polarisation can inform on the orientation of structures in a sample that are smaller than the diffraction limit. Among other things, this has been used to measure how the structure of DNA changes when it is subject to a strong stretching force, how integrin proteins respond to an applied force and measure the order of molecules embedded in the cell membrane, among others [2, 4, 5, 3]. In this section, I will first introduce the concept of light polarisation, then discuss how it can be used in a microscope, and finally mention some optical components that affect the light polarisation, which are crucial to conducting a polarisation microscopy experiment.

The polarisation ellipse. Remember that light is a transverse electromagnetic wave. This means that there are oscillations of the electric and magnetic fields along the path of a light ray, and that these oscillations are orthogonal to the propagation direction. In other words, if the light propagates along $\vec{k}$, the electric and magnetic fields $\vec{E}$ and $\vec{B}$ must satisfy $\vec{E} \cdot \vec{k} = \vec{B} \cdot \vec{k} = 0$. (The fields themselves are also orthogonal to each other, so we can neglect $\vec{B}$ without compromising our analysis.)

For the sake of simplicity, let's consider a ray propagating in the z direction. The electric field at any point in space and time can be written as

$$E_x(z,t) = E_{0x}\cos(kz - \omega t + \phi_x), \tag{1.1}$$
$$E_y(z,t) = E_{0y}\cos(kz - \omega t + \phi_y). \tag{1.2}$$

Polarisation state	E_{0x}	E_{0y}	δ	Jones vector
Linear along x	1	0	any	$(1, 0)$
Linear along y	0	1	any	$(0, 1)$
Linear at 45°	1	1	0	$(1, 1)$
Circular (left-handed)	1	1	$\pi/4$	$(1, i)$
Circular (right-handed)	1	1	$-\pi/4$	$(1, -i)$

Table 1.1: List of a number of polarisation states.

where $\vec{E}_0$ is the amplitude of the oscillation, k is the wavenumber (the length of $\vec{k}$), ω is the radial frequency and ϕ is an arbitrary phase. Note that the wavenumber and the frequency are related to each other through the speed of light c, since $\omega = kc$. Note that the x and y components can have a phase difference.

Letting $\delta = \phi_y - \phi_x$, it can be shown that

$$\left(\frac{E_x}{E_{0x}}\right)^2 - 2\cos\delta\frac{E_x}{E_{0x}}\frac{E_y}{E_{0y}} + \left(\frac{E_y}{E_{0y}}\right)^2 = \sin^2\delta. \tag{1.3}$$

This is the equation for an ellipse. That means that, at any point in time, the point (E_x, E_y) lies on the ellipse defined by the equation above, which is called the polarisation ellipse. The ellipse is characterised by E_{0x}, E_{0y} and δ:

- if $E_{0x} = 0$, the ray is said to be linearly polarised in the y direction, and vice versa,
- if neither are equal to 0, but they are in phase (meaning $\delta = 0$), the light is still polarised, at an angle $\psi = \arctan(E_{0y}/E_{0x})$ to the x axis,
- if the amplitudes in x and y are equal, and $\delta = \pm\pi/4$, then the light is circularly polarised. If *delta* is positive (negative), the polarisation is said to be right-handed (left-handed). (replace this list by table)

In general, the polarisation ellipse can be defined by means of two angles: the orientation ψ and ellipticity χ, as shown in (figure of pol ellipse from field guide to polarisation). They can be calculated from $\alpha = \arctan(E_{0y}/E_{0x})$ and the phase difference δ using

$$\tan 2\psi = \tan 2\alpha\cos\delta, \tag{1.4}$$

$$\sin 2\chi = \sin 2\alpha\sin\delta. \tag{1.5}$$

Microscopy. Why is this relevant to microscopy? Well, since a fluorophore can be considered a small dipole moment, the absorption of excitation light that is linearly polarised along an angle ψ will depend on the dipole orientation θ. The intensity of light emitted by that fluorophore will then satisfy

$$I(\psi, \theta) \propto \cos^2(\psi - \theta). \tag{1.6}$$

This is Malus's law. Analogously, light emitted from a fluorophore is always linearly polarised parallel to its dipole. One can place a linearly polarising filter in front of the detector to measure a fluorophore's orientation. If the polariser emits light polarised at an angle ψ, then the intensity measured at the detector also follows Malus's law, meaning that these two setups are analogous (not taking into account depolarisation effects in an experimental setup). As an example, see (figure of sir actin from spira2017).

Jones calculus. To finish this section, I'd like to introduce Jones calculus. This is an incredibly useful way to model light polarisation, as well as how it interacts with certain optical components that are present in our system, but it does require us to express the the electric field with a complex function. Let us express it as follows:

$$\vec{E}(z, t) = \vec{E}_0 e^{i(kz - \omega t)}. \tag{1.7}$$

In the following analysis, we will treat $\vec{E}$ as a two-dimensional vector with only an x and y component, as $E_z = 0$. Note that complex numbers are just a mathematical trick. The Maxwell equations that govern light propagation are linear, and taking the real part of a complex-valued function is also a linear

operation, so the complex extension of $\vec{E}$ will behave exactly the same as the actual electric field would. The phase difference between the two components is now contained in $\vec{E}_0$, which looks like

$$\vec{E}_0 = \begin{pmatrix} E_{0x} \\ E_{0y}e^{i\delta} \end{pmatrix}. \tag{1.8}$$

The Jones vectors for some special polarisation states are listed in Table 1.1.

The usefulness of Jones calculus lies in its ability to represent optical components as matrices acting on this vector. For example, a polariser that transmits x-polarised light has the following matrix form:

$$S_p = \begin{pmatrix} 1 & 0 \\ 0 & 0 \end{pmatrix}. \tag{1.9}$$

It is easy to verify that $S_p\vec{E}_0 = E_{0x}$. (ref further along with rotated components to prove malus' law) We also need to take into account how mirrors affect polarisation. A mirror flips the field component that is orthogonal (the s-component) to the mirror surface, while keeping the other component (p) unchanged. So, a mirror whose surface is parallel to the x-axis has a Jones matrix of the form

$$S_{mx} = \begin{pmatrix} 1 & 0 \\ 0 & -1 \end{pmatrix}. \tag{1.10}$$

Another important type of optical component in our setup is a waveplate. Waveplates or phase retarders are birefringent crystals, meaning the index of refraction a ray of light experiences is dependent on its polarisation. This happens when a crystal structure is not symmetric. (what kind of symmetry?) In these crystals, Equation 1.7 is no longer valid and should be substituted by

$$\vec{E}(z,t) = \begin{pmatrix} E_{0x}e^{i(k_x z - \omega t)} \\ E_{0y}e^{i(k_y z - \omega t + \delta)} \end{pmatrix}, \tag{1.11}$$

assuming the optical axes of the waveplate are along x and y. This can also be written as

$$\vec{E}(z,t) = \begin{pmatrix} E_{0x} \\ E_{0y}e^{i(\Gamma(z)+\delta)} \end{pmatrix} e^{i(k_x z - \omega t)} \quad \text{, where} \quad \Gamma(z) = (k_y - k_x)z. \tag{1.12}$$

As one can see, a waveplate only imparts a delay on the y-component of a beam, depending on its thickness z and its birefringence. We can neglect the common phase factor and represent the action of a waveplate by the following Jones matrix,

$$S_\Gamma = \begin{pmatrix} 1 & 0 \\ 0 & e^{i\Gamma} \end{pmatrix}. \tag{1.13}$$

Generally, waveplates are characterised by the relative delay they impart on the slowly propagating polarisation component. Quarter-wave plates delay it by a quarter of a wavelength compared to the fast propagating ray, corresponding to $\Gamma = \pi/2 + 2n\pi$ (for any integer n). Therefore, the Jones matrix of a quarter-wave plate satisfies

$$S_{\lambda/4} = \begin{pmatrix} 1 & 0 \\ 0 & i \end{pmatrix}. \tag{1.14}$$

Let's consider what happens to some specific cases. If vertically or horizontally polarised light passes through a quarter-wave plate, its polarisation will not change. But light polarised along $+45°$ ($-45°$) will be turned into left-handed (right-handed) light, and vice versa. Therefore, a quarter-wave plate allows us to convert between linearly and circularly polarised light. (figure of waveplate actions)

The second type of waveplate we should treat is a half-wave plate. It features a delay of $\Gamma = \pi + 2n\pi$, and its Jones matrix looks like

$$S_{\lambda/2} = \begin{pmatrix} 1 & 0 \\ 0 & -1 \end{pmatrix}, \tag{1.15}$$

which corresponds to mirroring the polarisation state along the x-axis. Another way to think about that is that a ray polarised along an angle ψ will be rotated by an angle -2ψ. Circularly polarised light will get the opposite handedness.

As said before, the power of Jones calculus lies in its ability to model the behaviour of a sequence of optical elements at arbitrary rotations. First, we need to define the Jones matrix for a rotated component. This is simply

$$S(\theta) = R(\theta) \cdot S \cdot R(-\theta) \quad \text{, where} \quad R(\theta) = \begin{pmatrix} \cos\theta & -\sin\theta \\ \sin\theta & \cos\theta \end{pmatrix} \quad \text{(check!)} \tag{1.16}$$

and θ is the angle of the component's x'-axis with the lab coordinate system's x-axis. (introduce). As an example, let's recover Malus's law by sending linearly polarised light through a half-waveplate at an angle $\theta/2$ (such that the light is polarised along θ after it) and then through a polariser.

$$I(\theta) \propto \left| S_p(0) \cdot S_{\lambda/2}(\theta/2) \cdot \begin{pmatrix} 1 \\ 0 \end{pmatrix} \right|^2 = \cos^2 \theta. \tag{1.17}$$

To do

- Moeller calc
- Hinting at psted

1.3. Super-resolution microscopy

2

Results (outline)

2.1. Validating the laser modules

For every laser in the setup (561 nm, 640 nm, and 775 nm), I measured the polarisation state of the light at different points in the beam path and at the sample plane, by measuring the power transmitted by a linearly polarising filter at different angles relative to the beam. At the sample location, the 640 nm beam is quite well-polarised when set to a linear polarisation. When rotating a polariser, the transmitted power drops to about one fifth of the maximum. At the circular setting, though, the light is quite elliptical, with a minimum power transmitted through the polariser being about half as bright as the maximum, see Figure C.1. The quality of the 561 nm polarisation is higher. When set to a linear polarisation, the power transmitted through a polariser drop from about 25 µW to a value almost equal to background levels around 0.1 µW, while the amplitude variations of the circularly polarised light are withing 14% of the mean, see Figure C.2. In conventional STED, the depletion beam is circularly polarised in order to achieve polarisation-independent quenching, so I also measured its polarisation state, see Figure C.3. The minimum power transmitted is about 63% of the max. (Calculate ellipticity angle, or introduce the E_{max}/E_{min} characteristic in the beginning.) (Put this stuff into a table?) (The fact that Emax/Emin is not amazing can be explained by depolarising effects of elements in the beam path)

There are two other things we can take away from those figures: the power of the 640 nm laser is not very constant. This can be explained by a slow ramp up to the set power every time the laser is turned on. Secondly, the noise on the signal from the 640 laser is higher. I believe this is due to the same effect. Therefore, I also measured the power profiles of the different lasers, see (figure). The conclusion from those measurements is that the response of the lasers to the desired power set in software is not linear at low powers. If experiments need to be done at low power, a neutral density filter is required. This is luckily not the case for biological specimens with a low density of fluorophores.

Finally, we also measured the PSFs of the different lasers as a sanity check. This is shown in Figure C.4. This data looks good. (Why does it look good?) (Mention how we got this data: PMT and gold beads.)

2.2. Validating the detection module

First off, I checked the polarisation dependence of the APDs. To do so, I ensured the light coming into the APDs was unpolarised by illuminating a sample of TetraSpec beads with circularly polarised 561 nm light, since that was the closest to circular that we could get. Then I put a polarising filter after the detection waveplates and measured the signal from the APD as a function of the incoming polarisation, see Figure C.5. For both APDs, there is a difference of about 4%.

To do:

- Should I do min/max like before? That would also be closer to a G factor, I guess.
- APD2 and power meter pol sensitivity.
- Correct for ellipticity of 561 polarisation

Second, I tested the effect of the detection waveplates on the polarisation state of incoming light. Linearly polarised input light was achieved by putting a polariser (P1) in the sample location and illuminating it with the microscope's top lamp. Then the intensity was measured by the APDs, which was dependent on the angle of a polariser located after the last waveplate (P2). Using Jones calculus, we

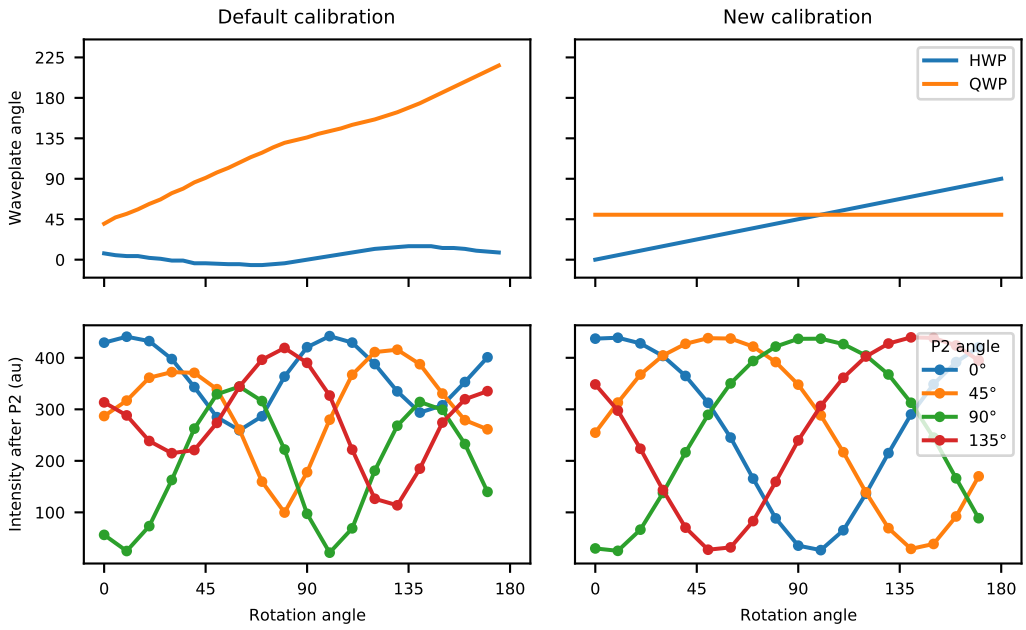

Figure 2.1: (text)

know that two QWPs and a HWP can form a proper polarisation rotator (ref methods), but the default calibration (a function that maps the total rotation angle to the angles the waveplates have to take on) is unable to do so. I determined that a better calibration sets the (non-fixed) QWP to an angle of 50° and the HWP to half the rotation angle. The angle of the QWP was chosen such that it is aligned with the fixed QWP at the microscope end. The behaviour of both calibrations is shown in Figure 2.1. The new calibration works as expected.

Finally, I also measured the polarisation characteristics of the POL cube. I generated linearly polarised light as in the previous paragraph, but left out P2. Then I rotated the polarisation using the detection waveplates and measured the intensity of light reflected and transmitted by the POL cube into APD1 and APD2 respectively. Apparently, the degree to which the POL cube can split the signal is strongly dependent on the polarisation of the light at the sample (the angle of P1), Figure 2.2. The cause of this effect is not immediately obvious, but is most likely due to some birefringence present in the POL cube. (Is that true?)

2.3. Demonstration of conventional polarisation microscopy

See Figure 2.3. To do:

- Colour wheels in the images
- sSTED + polarisation
- Can I get some quantitative results? (e.g. histograms of orientation/degree of polarisation, weighted by intensity)

2.4. Polarisation-resolved STED microscopy

(Refer back to the setup described in Methods.) The first step is to manipulate the polarisation of the depletion beam. Then I can do experiments on unpolarised and polarised controls (beads and Yersinia samples).

To get control of the light polarisation, the first step was to mount the new waveplates in the beam path. They were mounted after the SLM. The HWP was mounted inside a rotational stage and the QWP went in a cage system attached to the rotational stage, such that it is always aligned with the HWP, but its rotational angle is fixed. The first step was to find the angle of the QWP that maximised the linearity of the light polarisation at the sample. This was simply done by placing a polariser and a power meter at the sample and rotating them to characterise the polarisation of the depletion beam. I did this a couple of times, from which we concluded that the optimal angle for the QWP was 15°. (Does

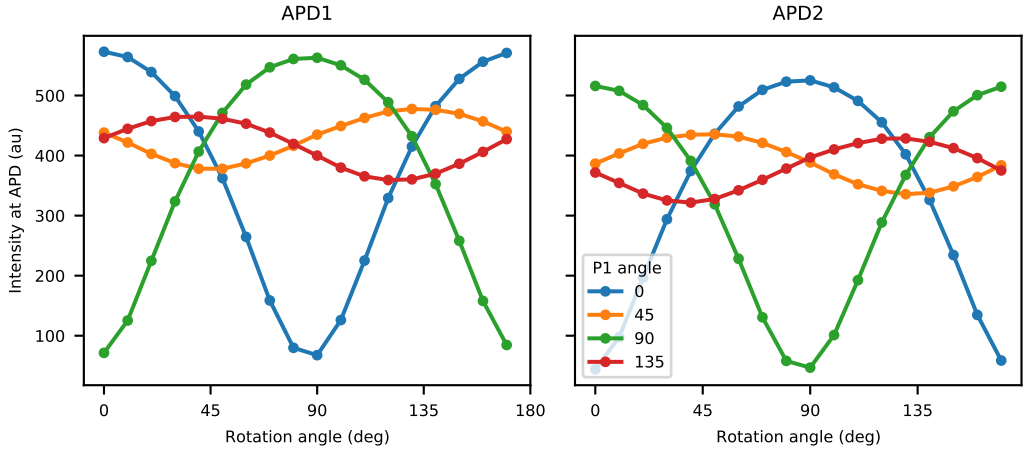

Figure 2.2: The POL cube distorts the polarisation state of incoming light. APD should measure the vertical component of the light (reflected by the POL cube), and APD2 should measure the horizontal component (transmitted). The detection waveplates were used to rotate incoming light, which was polarised along an angle shown in the legend.

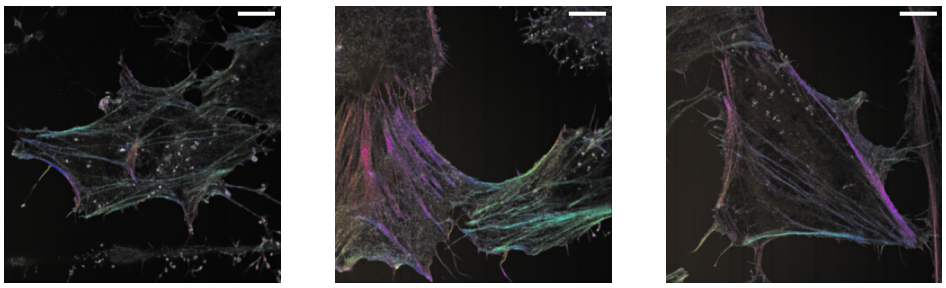

Figure 2.3: Polarisation microscopy images of three different cells. Scale bars 10 μm.

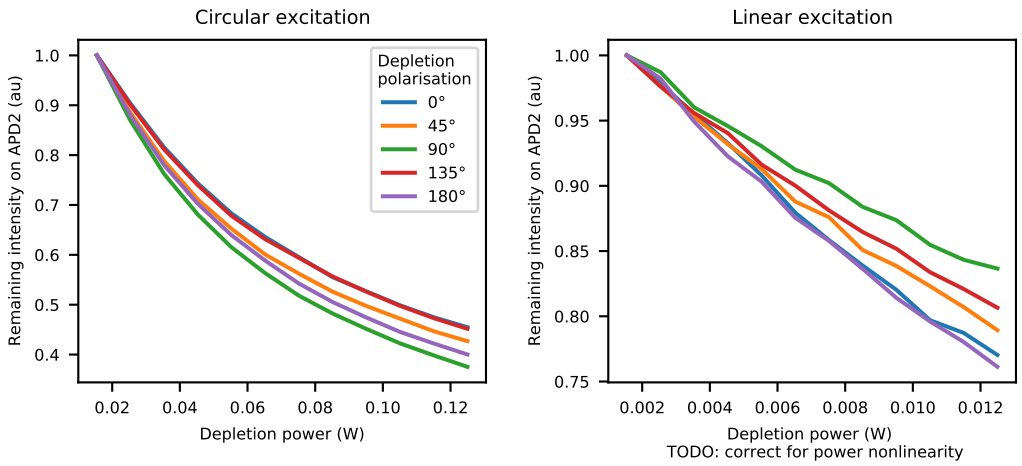

Figure 2.4: Dependency of surviving fluorescence on intensity and polarisation of depletion beam. **Left:** circular excitation. **Right:** linear excitation at 0° (vertical). (Maybe I should do a couple of repeats here, to make the figures more clear.)

this warrant a figure? I'm not sure it's necessary.) Next, I had to find the angle of the HWP at which the depletion beam is vertically polarised. In that position, the depletion beam has a polarisation parallel to the excitation lasers (at 0°). This turned out to be 38.4°. See Figure C.6.

Now that we have control over the beam polarisation, we can check how the added waveplates influence the PSF. In (figure), the PSF is shown for different polarisation directions. There are a number of conclusions we can draw from this data. Firstly, the PSF is not circular any more, even though the SLM was set to Gaussian mode. In particular, the ellipse orientation is parallel to the light polarisation, so we see the PSF rotating in sync with the light polarisation. This can be explained by the fact that a lens interacts differently with light polarised along different directions. This is why we would usually use circularly polarised light instead.

Other effects of the polarisation include the following: the intensity of the depletion beam varies as a function of the polarisation angle. This is probably due to linear dichroism present in the optical elements between the waveplates and the sample. That is to be expected, but should be accounted during either image acquisition or analysis. Furthermore, the eccentricity of the ellipse has a slight dependency on the polarisation angle, and the maximum of the PSF moves a little: up to (?) nm from its mean position. Fortunately this is a quite a bit below the diffraction limit for 775 nm light, i.e. around 400 nm.

Fixed, non-polarised beads are a good control sample, since we can determine the polarisation of emitted light by selectively activating fluorophores of a particular orientation with the polarisation of the excitation light. That is called photoselection. (Remove this phrase if I discuss photoselection in Background.) When these beads are excited with circularly polarised light, fluorophores of all orientations should be activated equally, and the polarisation of the depletion beam should not matter. In the case of linearly polarised excitation light, on the other hand, depletion should be more efficient when its polarisation is aligned with the excitation beam. This can be verified by increasing the depletion power: when the beams are aligned, then the remaining fluorescence signal should drop faster than when they are not, as predicted by (ref equation from Background). Figure 2.4 shows that this is indeed the case. While there is some variation in the depletion rate under circular excitation, it can not be explained by the theory and seems random, unlike the case of linear excitation. There, depletion goes fastest when the beams are aligned, slower when there is a 45° angle between them, and slowest when they are orthogonal. If the depletion beam was even more linearly polarised (instead of Emin/Emax=.2), then this effect would be even more pronounced.

(pSTED results in cells.)

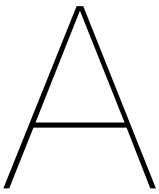

References

[1] Arbetsmiljöverket. *Artificiell optisk strålning, Arbetsmiljöverkets föreskrifter om artificiell optisk strålning och allmänna råd om tillämpningen av föreskrifterna*. https://www.av.se/globalassets/filer/publikationer/foreskrifter/artificiell-optisk-stralning-foreskrifter-afs2009-7.pdf. Accessed: 2021-03-15. 2019.

[2] Adam S. Backer et al. "Single-molecule polarization microscopy of DNA intercalators sheds light on the structure of S-DNA". In: *Science Advances* 5.3 (2019). ISSN: 23752548. DOI: 10.1126/sciadv.aav1083.

[3] Sophie Brasselet et al. "Imaging Molecular Order in Cell Membranes by Polarization-Resolved Fluorescence Microscopy". In: *Fluorescent Methods to Study Biological Membranes*. Berlin, Heidelberg: Springer Berlin Heidelberg, 2013, pp. 311–337. ISBN: 978-3-642-33128-2. DOI: 10.1007/4243_2012_51. URL: https://doi.org/10.1007/4243_2012_51.

[4] Pontus Nordenfelt et al. "Direction of actin flow dictates integrin LFA-1 orientation during leukocyte migration". In: *Nature Communications* 8.1 (2017). ISSN: 20411723. DOI: 10.1038/s41467-017-01848-y. URL: http://dx.doi.org/10.1038/s41467-017-01848-y.

[5] Vinay Swaminathan et al. "Actin retrograde flow actively aligns and orients ligand-engaged integrins in focal adhesions". In: *Proceedings of the National Academy of Sciences of the United States of America* 114.40 (2017), pp. 10648–10653. ISSN: 10916490. DOI: 10.1073/pnas.1701136114.

(Improve bibstyle)

B

A note on laser safety

The 775 nm line is a class 4 laser source. Under normal operation, the user is protected from it. However, when calibrating the STED beam or placing new components in the beam path, it is theoretically possible for the collimated laser beam to be reflected into the user's eyes. A high-powered laser beam can do permanent damage to the skin and retina, so we have to make sure we stay below the limits imposed by the Work Environment Agency's (Arbetsmiljöverkets) limits [1]. These regulations set forth three main conditions to calculate the Maximum Permissible Exposure (MPE) of a pulsed laser, see table 2.6 of the regulations. Important values and formulas about our setup, as well as the limits provided by the Work Environment Agency are provided in Table B.1 and in the text below.

Table B.1: Operating characteristics of the 775 laser line and relevant safety parameters.

Quantity	Symbol	Value
Beam radius	r	0.5 mm
Pulse width (FWHM)	τ	1.3 ns
Pulse repetition frequency	f	40 MHz
Pulse energy	E_{pulse}	31 nJ
Average power	P_{avg}	1.25 W
Thermal correction time	T_{min}	18 µs
Ca	C_a	1.41
Cc	C_c	1
Ce	C_e	1

Rule 1: The dose of a single pulse must not exceed the single-pulse MPE. The pulse dose H_{pulse} of the 775 nm laser at full power is

$$H_{pulse} = \frac{E_{pulse}}{2\pi r^2} \approx 39\,\mathrm{mJ/m^2}, \tag{B.1}$$

whereas the MPE equals

$$H_{pulse}^{MPE} = 5 \times 10^{-3} C_a C_e = 7.1\,\mathrm{mJ/m^2}. \tag{B.2}$$

This formula is found in table 2.2 of the regulations.

Rule 2: The dose of a single pulse may not exceed the thermally-corrected MPE. This weighs the pulse MPE with the amount of pulses in an interval T_{min}. The number of pulses in such an interval is $n = f \cdot T_{min}$, so

$$H_{thermal}^{MPE} = n^{-1/4} H_{pulse}^{MPE} = 1.3\,\mathrm{mJ/m^2}. \tag{B.3}$$

Rule 2 is therefore more strict than the rule 1. For safe operation, the laser must be ran at a power below 3.3% ($= H_{thermal}^{MPE}/H_{pulse}$).

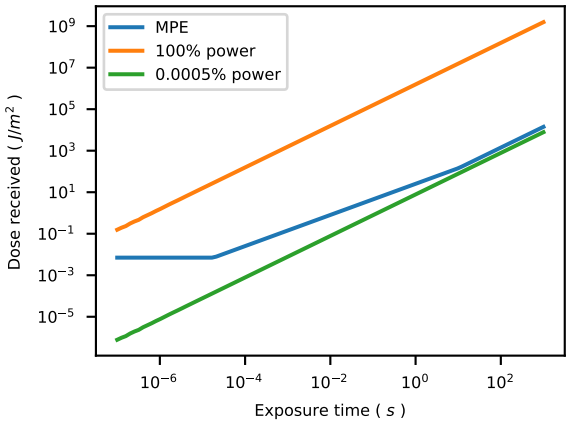

Figure B.1: Maximum permissible and actual exposure to the collimated STED beam as a function of exposure time.

Rule 3: The cumulative dose for a group of pulses in an interval of time t must not exceed the MPE for a single pulse of that time. Taking the necessary values from tables 2.2 and 2.3, the cumulative MPE is defined as

$$H_{tot}^{MPE}(t) = \begin{cases} 5 \times 10^{-3}\, C_a C_e & t < 18\,\mu\text{s}, \\ 18 t^{0.75}\, C_a C_e & 18\,\mu\text{s} < t < 10\,\text{s}, \\ 10 t\, C_a C_c & t > 10\,\text{s}. \end{cases} \tag{B.4}$$

The actual dose, on the other hand, is

$$H_{tot}(t) = \lfloor ft \rfloor H_{pulse}, \tag{B.5}$$

where $\lfloor \cdot \rfloor$ is the flooring function. This function is plotted in Figure B.1, from which it can be seen that the laser is only safe to use at 0.0005% capacity. Since the minimum laser power offered by the software is .05%, OD2 goggles should be worn to guarantee safe operation of the 775 nm laser.

C

Supplemental figures

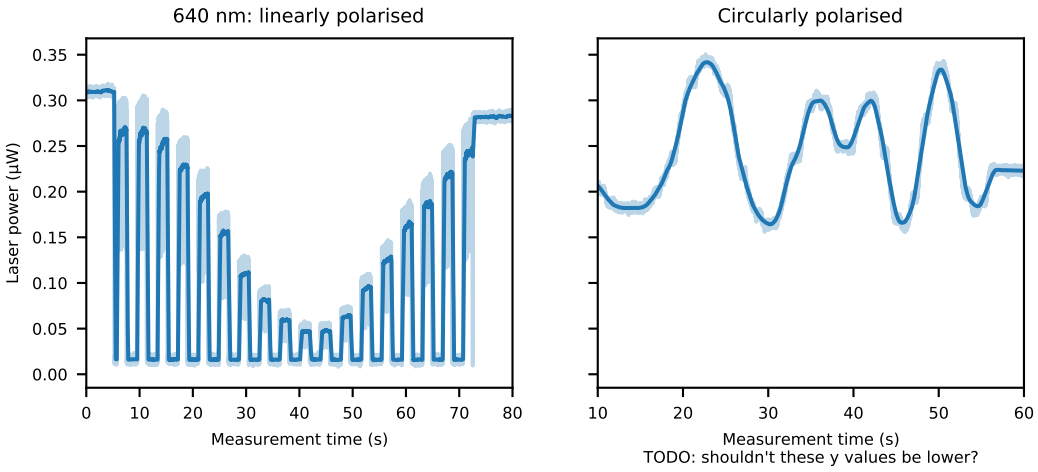

Figure C.1: Polarisation characteristics at the sample plane of the 640 laser. **Left:** power transmitted through a stationary polariser aligned to maximise transmission of the 640 laser set to an polarisation of 0° (vertical in the sample plane), while the laser beam rotates. **Right:** power transmitted through a manually rotating polariser, while the beam is set to circular polarisation.

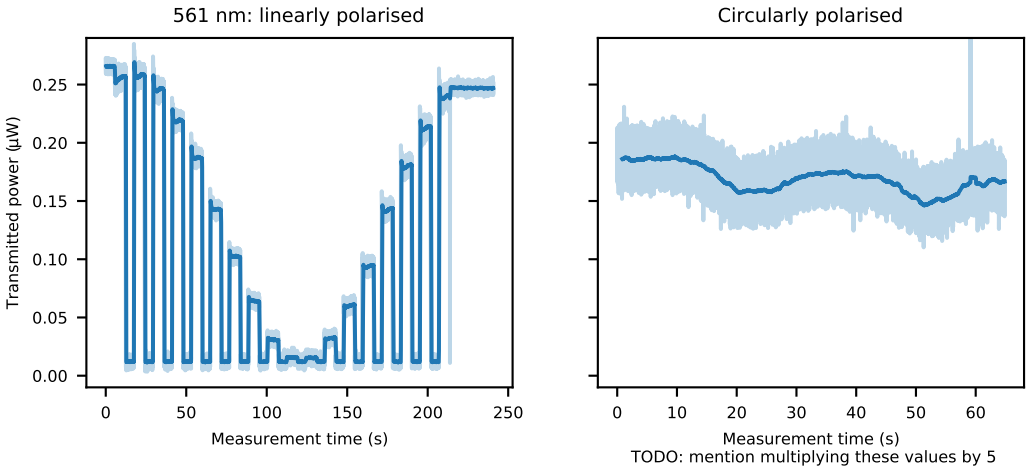

Figure C.2: Polarisation characteristics at the sample plane of the 561 laser. Left and right panes are the same as Figure C.1. (As the data on the left was acquired at 50% laser power to increase the signal at minimum transmission, but the data on the right was acquired at 10% laser power for safety reasons, the data on the right has been multiplied by a factor of 5 to allow comparison between the two figures. This also increased the noise.)

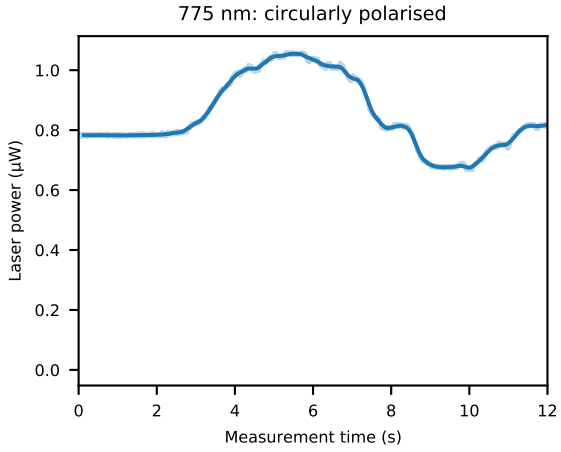

Figure C.3: Polarisation characteristics at the sample plane of the depletion beam, without pSTED optics. As its polarisation state cannot be manipulated through the software, only circular polarisation is characterised by manually rotating a polariser at the sample plane and measuring the transmitted power.

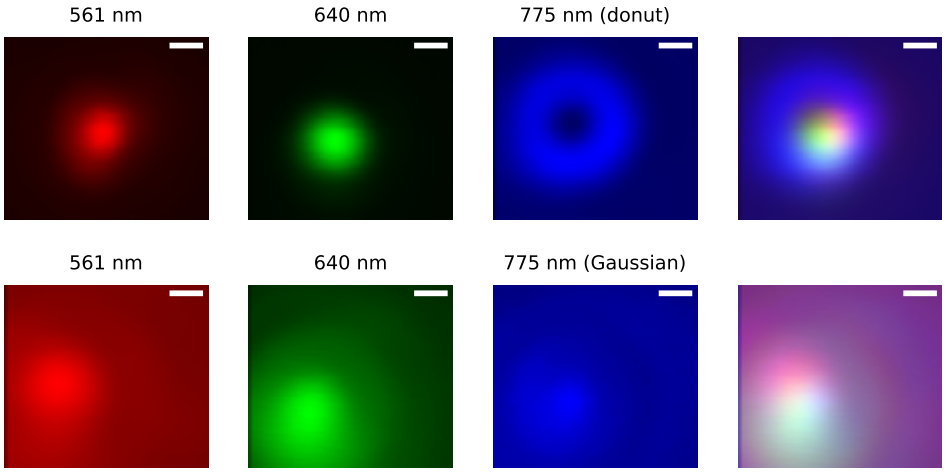

Figure C.4: Point spread functions of the different lasers at different SLM configurations, by measuring the reflection from 100 nm wide gold beads. Scale bars 200 nm. (show better data from 26 march)

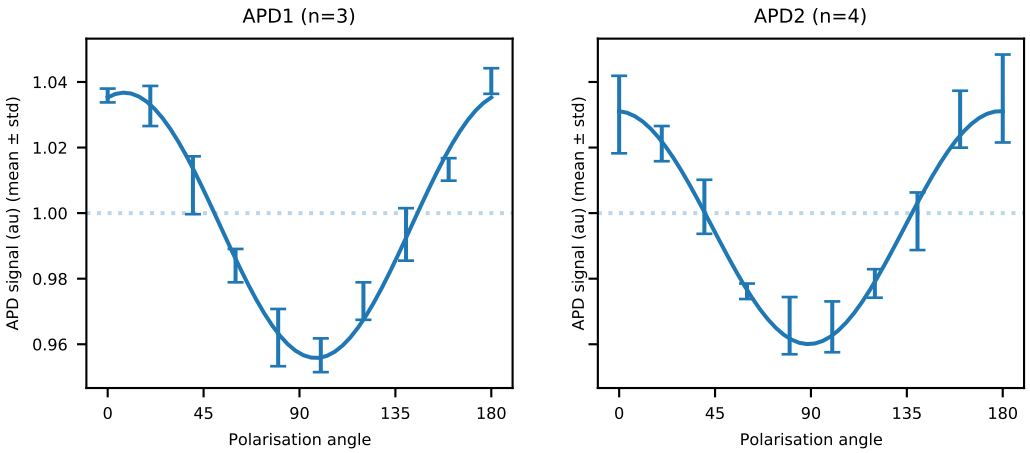

Figure C.5: Dependence of the signal from APD1 on the angle of polarisation of incoming light.

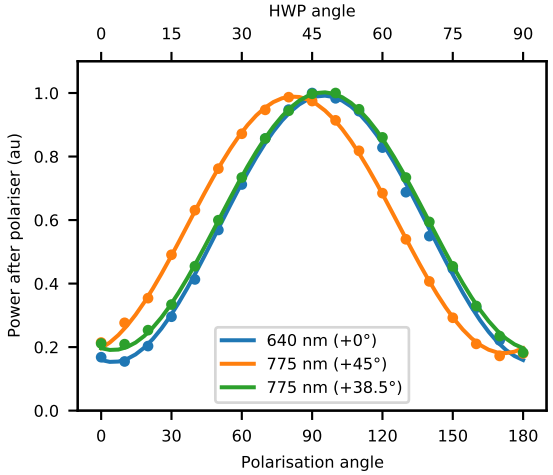

Figure C.6: The rotating HWP I put in the beamline controls the depletion beam polarisation. With an offset of 38.4°, the depletion beam is parallel to the 640 laser (set to vertical linear polarisation).